

Article

Application of the Molecular Interaction Volume Model for Calculating Activities of Elements in Ferromanganese Alloys: Mn-C, Mn-Fe, Fe-C, and Mn-Fe-C Systems

Haipeng Chen, Lihua Gao ^{*}, Wenlong Zhan , Zhijun He and Junhong Zhang ^{*}

School of Materials and Metallurgy, University of Science and Technology Liaoning, Anshan 114051, China; chenhaipengustl@163.com (H.C.); zhanwenlong288@163.com (W.Z.); hezhijun@ustl.edu.cn (Z.H.)

^{*} Correspondence: gaolihua@ustl.edu.cn (L.G.); zhangjunhong@ustl.edu.cn (J.Z.)

Abstract: The molecular interaction volume model (MIVM) developed by Tao is a fluid-based model derived from statistical thermodynamics and fluid phase equilibria. The MIVM was applied successfully to predict each element's activity in Mn-based alloys, namely, Mn-C Mn-Fe, and Mn-Fe-C systems. The MIVM calculated binary parameters between metals (Fe, Mn) and nonmetal (C) in Mn-Fe-C alloys, confirming a strong interaction between Fe and Mn in Mn-Fe-C alloy. The MIVM indicated that iron has a great influence on the activity of Mn and little effect on the activity of carbon. A significant advantage of MIVM is its ability to explain the experimental phenomenon in the Mn-Fe-C ternary system, whereby the predicted values are in good agreement with the experimental data, showing that this model is reliable, convenient, and economic.

Keywords: thermodynamics; manganese; activity; molecular interaction volume model



Citation: Chen, H.; Gao, L.; Zhan, W.; He, Z.; Zhang, J. Application of the Molecular Interaction Volume Model for Calculating Activities of Elements in Ferromanganese Alloys: Mn-C, Mn-Fe, Fe-C, and Mn-Fe-C Systems. *Crystals* **2022**, *12*, 682. <https://doi.org/10.3390/cryst12050682>

Academic Editors: Yufeng Guo, Shuai Wang, Mao Chen, Kexin Jiao, Lingzhi Yang, Feng Chen and Fuqiang Zheng

Received: 28 March 2022

Accepted: 29 April 2022

Published: 9 May 2022

Publisher's Note: MDPI stays neutral with regard to jurisdictional claims in published maps and institutional affiliations.



Copyright: © 2022 by the authors. Licensee MDPI, Basel, Switzerland. This article is an open access article distributed under the terms and conditions of the Creative Commons Attribution (CC BY) license (<https://creativecommons.org/licenses/by/4.0/>).

1. Introduction

High-purity ferromanganese alloys have great potential in applications as structural components in the automotive industry, such as for transformation-induced plasticity (TRIP) and twinning-induced plasticity (TWIP), due to their excellent tensile strength and ductility properties as a result of their face-centered cubic austenitic structure [1,2]. The development of these materials requires a full understanding of the thermodynamic stability of the phase constituting the binary Mn-C and ternary Mn-Fe-C systems. In order to predict the smelting limit of C, a fundamental understanding of thermodynamic behavior of elements in ferromanganese alloy was essential to assess the thermodynamic information of the liquid solution in Mn-based alloys, as well as reduce the evaporation of manganese [3–6]. However, the use of molten Mn-C and Mn-Fe-C in liquid molten alloy presents significant challenges in that the high smelting temperature of Mn, Fe, and C requires a high operating temperature (1355–1500 °C) at various low CO pressures (P_{CO}). The present study was aimed at establishing a thermodynamic model of element behavior in Mn-based alloys, which may be used as a predictive tool for a wide range of conditions pertaining to the refining of these alloys [7,8].

The thermodynamic properties of ferromanganese alloys have previously been experimentally and theoretically investigated using Mn-C and Mn-Fe-C liquid alloys [2–14]. Wagner's interaction parameters have been widely used for the evaluation of activity of components in Mn-based melts, but they have limitations for multicomponent systems [5]. The unified interaction parameter formalism (UIPF) [10] developed by Bale and Pelton [15,16] was even able to predict the thermodynamic properties of a quaternary system (Mn-Fe-Si-C), but the Mn-based and Fe-based interaction parameters using UIPF showed significant differences [17]. The phase equilibria and thermodynamic properties in binary Mn-C alloy and ternary Mn-Fe-C alloy were assessed using phase diagrams, show-

ing a negative or positive deviation with experimental data across the whole composition range [2,4,11,18].

In previous work, the molecular interaction volume model (MIVM) developed by Tao was shown to be capable of modeling the thermodynamic properties of most alloy systems [19–25]. As the MIVM is derived from statistical thermodynamic and fluid phase equilibria, it has the advantage in that its formulation does not require assumptions regarding the composition of an element as solute or solvent, and it uses fewer fitting parameters, which enables better stability and reliability when predicting the activity coefficients of binary and multicomponent alloy systems across the whole composition range [19]. Tao showed that his model could be used to predict the properties of multicomponent systems [20]. The study presented in this paper is part of a project aimed at providing a precise and reliable thermodynamic model of MIVM which predicts the thermodynamic properties of binary (Mn-C) and ternary (Mn-Fe-C) alloys.

2. Molecular Interaction Volume Model (MIVM)

The molecular interaction volume model (MIVM) developed by Tao is a fluid-based model derived from statistical thermodynamics and fluid phase equilibria [19]. The MIVM was fitted to experimental data using two parameters to represent the molar and partial thermodynamic properties of the liquid solution. For the activity coefficients of i and j in a binary i - j alloy, γ_i and γ_j were derived as new expressions by Tao [19,24–26], introducing two pair potential energy interaction parameters, B_{ji} and B_{ij} .

$$\ln \gamma_i = \ln\left(\frac{V_{mi}}{x_i V_{mi} + x_j V_{mj} B_{ji}}\right) + x_j \left(\frac{V_{mj} B_{ji}}{x_i V_{mi} + x_j V_{mj} B_{ji}} - \frac{V_{mi} B_{ij}}{x_j V_{mj} + x_i V_{mi} B_{ij}}\right) - \frac{x_j^2}{2} \left(\frac{Z_i B_{ji}^2 \ln B_{ji}}{(x_i + x_j B_{ji})^2} + \frac{Z_j B_{ij} \ln B_{ij}}{(x_j + x_i B_{ij})^2}\right), \quad (1)$$

$$\ln \gamma_j = \ln\left(\frac{V_{mj}}{x_j V_{mj} + x_i V_{mi} B_{ij}}\right) - x_i \left(\frac{V_{mj} B_{ji}}{x_i V_{mi} + x_j V_{mj} B_{ji}} - \frac{V_{mi} B_{ij}}{x_j V_{mj} + x_i V_{mi} B_{ij}}\right) - \frac{x_i^2}{2} \left(\frac{Z_j B_{ij}^2 \ln B_{ij}}{(x_j + x_i B_{ij})^2} + \frac{Z_i B_{ji} \ln B_{ji}}{(x_i + x_j B_{ji})^2}\right), \quad (2)$$

where x_i and x_j are the molar fractions of components, Z is the input parameter as the first coordination number, and V_m is the molar volume in the alloy liquid state. The pair potential energy interaction parameters B_{ji} and B_{ij} are defined in Equation (3).

$$B_{ji} = \exp\left[\frac{-(\varepsilon_{ji} - \varepsilon_{ij})}{kT}\right], B_{ij} = \exp\left[\frac{-(\varepsilon_{ij} - \varepsilon_{jj})}{kT}\right]. \quad (3)$$

The coordination number Z_i of liquid metal can be predicted using Equation (4).

$$Z_i = \frac{4\sqrt{2\pi}}{3} \left(\frac{r_{mi}^3 - r_{m0}^3}{r_{mi} - r_{m0}}\right) \rho_i r_{mi} \exp\left(\frac{\Delta H_{mi}(T_{mi} - T)}{Z_c R T T_{mi}}\right), \quad (4)$$

where $\rho_i = N_i/V_i = 0.6022/V_{mi}$ is the molecular number density, ΔH_{mi} and T_{mi} are the melting enthalpy and temperature, respectively, $Z_c = 12$ denotes the close-packed coordination, T is the liquid metal temperature, and r_{m0} and r_{mi} are the values of the initial and first peak of radial distance in a radial distribution near the melting point, respectively. Specifically, r_{m0} may be fitted as proportion of the atomic covalent diameter, d_{covi} , which implies that a covalent bond length formed should share the outmost valence electrons with other atoms approaching the closest distance between adjacent atoms, whereas r_{mi} is approximated to the observed atomic diameter σ_i . Therefore, the following equation holds:

$$r_{oi} = 0.918d_{covi}, r_{mi} = \sigma_i. \quad (5)$$

Equation (5) is not suitable for nonmetal element C [17,24]. Its coordination number is calculated using the following equation:

$$Z_i = (Z_{is}Z_lZ_c)^{1/3} = (120Z_{is})^{1/3}, \quad (6)$$

where Z_{is} is the coordination number of element i in a solid state, $Z_l = 10$ is the coordination number of a liquid, and $Z_c = 12$ is the coordination number of a close-packed solid. Thus, $Z_{is} = 4$ for nonmetal C in a solid state, while $Z_c = 7.83$ in a liquid state. The required parameters for the pure components are listed in Table 1.

Table 1. Input parameters of the three elements in the MIVM.

i	V_{mi} (cm ³ ·mol ⁻¹)	ΔH_{mi} (kJ mol ⁻¹)	σ_i (10 ⁻⁸ cm)	d_{covi} (10 ⁻⁸ cm)
Mn	$9.54 \cdot [1 + 1.6 \times 10^{-4} \cdot (T - 1517)]$	14.6	2.61	2.34
Fe	$7.94 \cdot [1 + 1.3 \times 10^{-4} \cdot (T - 1808)]$	13.77	2.55	2.34
C	5.30	-	1.82	1.54

To determine the value of B_{MnC} and B_{CMn} in the Mn-C alloys, their component activities were fitted according to Equations (1) and (2) using the MIVM expression. The error of a_{Mn}/a_C was determined by calculating the minimal error. The activities of Mn and C in the alloy were obtained from appropriate references [7,8]. The error in Mn-C binary alloys was minimized using Equation (7) via a nonlinear least-square analysis; this iterative method was applied to optimize the interaction parameters using the numerical solver in Matlab.

To confirm that the solution for the interaction coefficients of B_{MnC} and B_{CMn} did not depend on the choice of initial values in the optimization process, the error (B_{MnC} and B_{CMn}) was plotted as a 3D graph. As seen in Figure 1 for the representative case of B_{MnC} and B_{CMn} , there was only one minimum in this function, and coordinates of this error value were calculated as a function of this minimum using the numerical solver in Matlab. Experimental data for the Mn-C alloy were sourced from extensive studies at 1628–1773 K [2–14]. To evaluate the goodness of fit, the error in the partial $a_{Mn,exp}^i$ and $a_{Mn,pre}^i$ was also calculated, as defined in Equation (7).

$$Error = \frac{1}{n} \sum_{i=1}^n \left| \frac{a_{Mn,exp}^i / a_{C,exp}^i - a_{Mn,pre}^i / a_{C,pre}^i}{a_{Mn,exp}^i / a_{C,exp}^i} \right|, \quad (7)$$

where $a_{Mn,exp}^i$ and $a_{Mn,pre}^i$ are the experimental data and the predicted activity values of component i by MIVM, respectively; a similar expression describing how $a_{C,exp}^i$ and $a_{C,pre}^i$ vary with component i indicates the minimized error of activity, and n is the number of experimental data points.

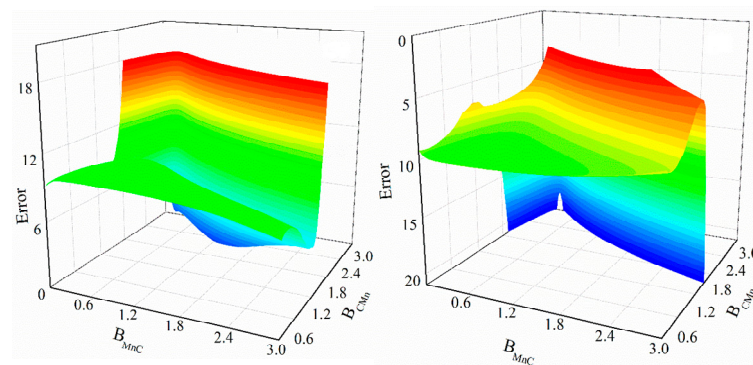


Figure 1. Representative case of error as a function of B_{MnC} and B_{CMn} in the case of Mn-C liquid alloy at 1772 K (minimum obtained for $B_{MnC} = 1.780$ and for $B_{CMn} = 1.343$).

3. Results and Discussion

3.1. Evaluation of B_{MnC} and B_{CMn} in Mn-C Binary System

The activity values of Mn-C binary alloy were measured using MIVM and sourced from previous work, as shown in Figure 2. The values were calculated for B_{ij} and B_{ji} at the specific temperatures listed in Table 2. In order to assess the goodness error of a_C and a_{Mn} , the activity of Mn and C in Mn-C binary alloys was calculated using different models [2–14]. In these studies, Kim et al. [7] and Katsnelson et al. [8] obtained their data from a variety of experimental measurements, whereas Paek et al. [4], Li et al. [10], Chen et al. [13], and Young et al. [12] calculated their model using previous data. Kim et al. [7] measured the variation in CO pressure as a function of temperature from 1673 K to 1773 K over a wide range of components X_C (0 to 0.3) using the Gibbs-Duhem equation, which was intergrated through Belton-Fruehan treatment. Katsnelson et al. [8] also measured and calculated the activity of Mn and C in Mn-C binary alloy using the Gibbs-Duhem equation, with $X_C = 0.114$ and 0.278 at 1673 K and 1638 K, respectively. Li et al. [10] utilized the unified interaction parameter model (UIPM) developed by Bale and Pelton to assess the activity coefficient of each component, as well as the solubility of carbon, in Mn-based alloys for the first time, showing a negative and a positive deviation from experimental data at 1773 K and 1673 K, respectively. Then, Young et al. [12,14] calculated the thermodynamic properties of Mn-C binary alloy using UIPF, showing a positive or negative deviation at a lower carbon concentration ($X_C < 0.15$) compared with experimental data. Peak et al. [4] and Dejan et al. [2] calculated phase diagrams of the Mn-C binary system, revealing that these data were not in particularly good agreement in the range of compositions studied ($X_C < 0.3$). Chen et al. [13] calculated the relationship between thermodynamic properties and specific temperatures in Mn-C systems, showing that the calculated values coincided with the experimental data; however, this method based on thermodynamic deviation and calculation cannot be easily extended to other alloys with multiple components. The error results of a_{Mn}/a_C are listed in Table 3 as the average relative error given by Equation (7). It can be seen for MIVM that most errors at various temperatures were much smaller than those for others models characterizing liquid alloy in the range of 1628 K to 1773 K. This demonstrates that the MIVM for Mn-C alloy is effective and reliable for predicting the activity values of each component.

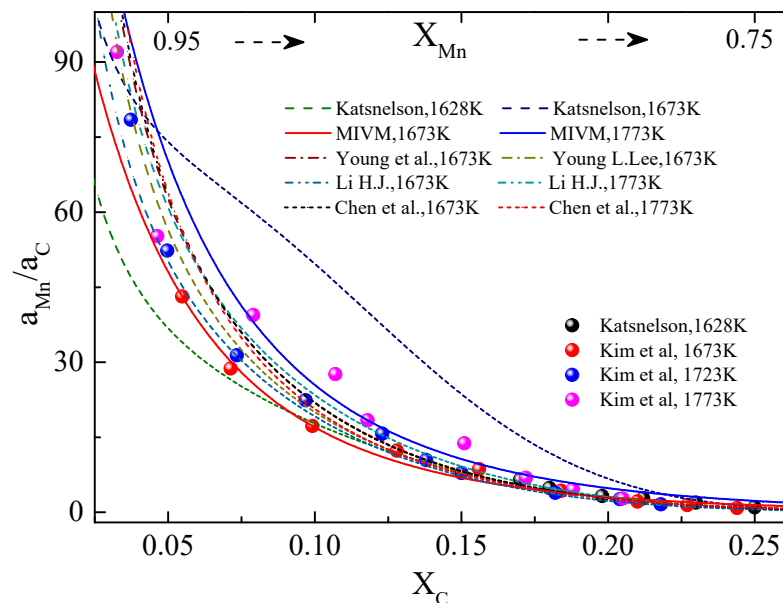


Figure 2. The calculated activity of Mn/C in Mn-C melt at 1673 K and 1773 K compared with experimental data.

Table 2. Calculated values of B_{MnC} and B_{CMn} using MIVM in Mn-C binary liquid alloys at 1628 K to 1773 K.

T(K)	B_{MnC}	B_{CMn}
1628	2.111	0.969
1673	1.809	1.201
1723	1.780	1.343
1773	1.679	1.703

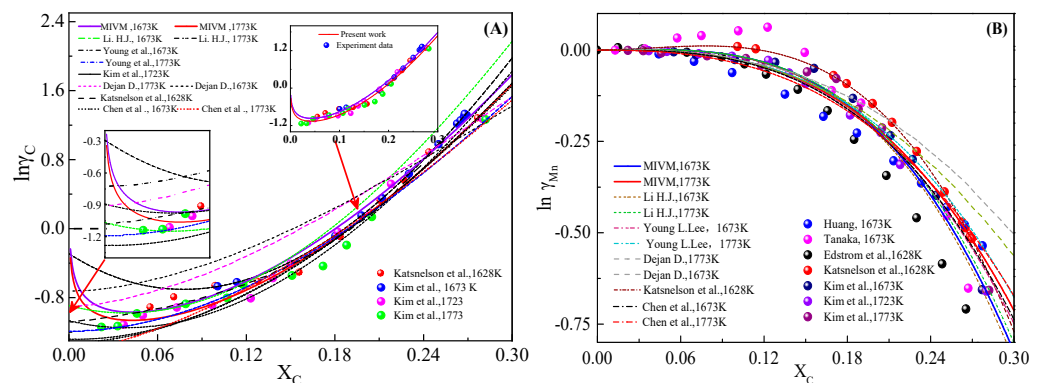
Table 3. Error comparison between experimental data in previous work and predicted values using different models for the pair potential interaction parameters in Mn-C liquid alloys at 1628 K to 1773 K (%).

Error	1628 K	1673 K	1723 K	1773 K
MIVM	5.19	4.10	3.23	5.56
Young et al.	6.29	5.38	4.62	6.94
Li et al.	6.35	5.46	3.64	6.83
Chen et al.	5.18	4.21	3.25	4.52
Katsnelson et al.	3.46	11.24	-	-

The $\ln\gamma_{Mn}-X_C$ and $\ln\gamma_C-X_C$ relationships were established at each temperature using Equations (1) and (2), as shown in Figure 3A,B. To evaluate the goodness of fit, the average errors in the partial Gibbs free energy of Mn and C are also indicated, as defined in Equation (8). A similar expression can be used to describe how the error (a_C) varies with composition.

$$Error(a_{Mn}) = \left(\sum_{i=1}^n (\ln(a_{Mn,exp}) - \ln(a_{Mn,pre}))^2 \right)^{1/2} / n \quad (8)$$

Yang et al. [22], Liu et al. [23], and Yan et al. [27] calculated the related binary parameters (B_{ij} and B_{ji}) using activity coefficients $\ln\gamma_i^\infty$ and $\ln\gamma_j^\infty$ of the binary liquid alloy using MIVM. The infinite dilution activity coefficients γ_i^∞ and γ_j^∞ of the binary liquid alloy were assessed when X_i and X_j approached zero, respectively. However, the related binary parameters of B_{MnC} and B_{CMn} for these components cannot be easily obtained using the above method, mainly due to the activity coefficient of carbon at infinite dilution (γ_C^∞) ($X_C \approx 0$). This coefficient was calculated in previous studies, showing significant distinctions (Figure 3A). In addition, at various experimental temperatures, the lowest equilibrium ultralow carbon content was $X_C = 0.022$ (2.93 wt.%) under ultralow CO partial pressure, resulting in inaccuracies when calculating γ_C^∞ in the low-carbon range.

**Figure 3.** $\ln\gamma_{Mn}$ (A) and $\ln\gamma_C$ (B) vs. X_C concentration in Mn-C liquid alloys at 1628 to 1773 K; experimental data are represented by symbols, while solid and dashed lines represent a_{Mn}/a_C modeled herein using the MIVM and other models, respectively.

The measured and estimated activity coefficients of $\ln\gamma_C$ and X_C for the Mn-C system are shown in Figure 3A. Katsnelson et al. [8] reported a significant positive deviation of manganese activity when compared with the results of Kim et al. [7] and Huang et al. [28], revealing worse fitting with the experimental data. Dejan et al. [2] calculated the relationship of $\ln\gamma_C$ and X_C using a phase diagram, showing a significant difference between calculated values and experimental data in the range of compositions studied ($X_C < 0.24$). The present assessment using MIVM agrees reasonably with most experimental data and other assessments. However, the activity coefficient of carbon at infinite dilution (γ_C^∞) ($X_C \approx 0$) showed significant distinctions in previous studies. The calculated activity coefficients of Mn in Mn-C alloy at temperatures ranging from 1628 K to 1773 K are compared with experimental data and other models in Figure 3B, showing both positive and negative deviations. The agreement between calculated and measured values using MIVM was satisfactory. The errors (a_{Mn} and a_C) in Mn-C liquid alloys are listed in Table 4 as the average relative error calculated using Equation (8). Compared with previous studies, the MIVM showed a significant advantage through its ability to predict the thermodynamic properties across the whole composition range using the binary activity coefficients of Mn-C alloys.

Table 4. Errors (a_{Mn} and a_C) in Mn-C liquid alloys at 1673 K and 1773 K calculated using different models or experimentally measured by Kim et al. at 1723 K and Katsnelson et al. at 1628 K.

Error (kJ/mol)	T/K	MIVM	Li et al.	Young et al.	Dejan et al.	Chen et al.	Kim et al. 1723 K	Katsnelson et al. 1628 K
Error (a_C)	1673 K	0.12	0.11	0.13	0.54	0.13	0.13	0.14
	1773 K	0.14	0.61	0.18	0.42	0.22		
Error (a_{Mn})	1673 K	0.59	0.71	0.64	0.78	0.60	0.56	0.61
	1773 K	0.65	1.12	1.23	0.95	0.86		

As shown in Figure 3A, this phenomenon may be partially attributed to experimental error at high Mn content. If the observed trend is representative of the thermodynamic properties of Mn-C alloy, it suggests that Mn-Mn interactions become more favorable than Mn-C interactions at high Mn content [20]. Figure 4 shows the environment of each atom in Mn-C binary alloy, where it appears that the environment of C is quite different from that of Mn. Therefore, this indicates that the interaction between Mn and C is probably affected by the strong interaction between Mn and its nearest neighbors in the range of compositions studied. This can explain why other models revealed a significant deviation at high manganese content. Therefore, the interaction parameters in MIVM are effectively dependent on the system composition [20]. A significant advantage of MIVM is its ability to explain the experimental phenomena at high Mn content in Mn-C binary systems. This shows that the MIVM with binary parameters is more effective and reliable than other models in predicting the Mn and C activities of binary systems in the range of given liquid compositions and temperatures.

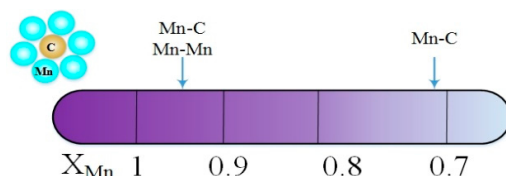


Figure 4. Environment of each atom in Mn-C binary alloys determined from MIVM modeling.

3.2. Mn-Fe Binary System: Evaluation of B_{MnFe} and B_{FeMn}

Thermodynamic modeling of the Mn-Fe system was performed by Huang [28], and the results are included in most commercial thermodynamic databases. Witusiewicz [29] investigated this system paying attention to the enthalpy of formation and heat capacity

of Mn-Fe alloys. Recently, Huang et al. [30] assessed the Fe-Mn binary liquid phase using the modified quasichemical model (MOM) in pair approximation. Li et al. [10] and Young et al. [12,14] reasonably assumed that Fe and Mn formed an ideal solution, whereby the first-order and second-order interaction parameters, ϵ_{FeFe} and ϵ_{FeFeFe} , were negligibly small and taken as zero. However, the thermodynamic behavior of manganese was not identical to that of iron, despite some similarities. The formation of Mn-Fe alloy resulted in a lower activity of manganese compared to pure manganese, with limited manganese vaporization losses [6]. Tao [19] showed that MIVM with binary parameters was more effective and reliable than UIPM in predicting the activities of all three components in the ternary system Mn-Fe-P. Furthermore, the thermodynamic parameters of the Fe-Mn binary liquid phase was determined using MIVM by establishing a relationship between B_{MnFe} and B_{FeMn} . According to Tao’s MIVM, the temperature dependence of B_{MnFe} can be described by $\ln(B_{MnFe}) = -(\epsilon_{MnFe} - \epsilon_{FeFe})/kT$, where ϵ_{MnFe} is the pair potential energy of a central Fe atom and its first nearest neighbor Mn. A similar expression can be used to describe how B_{FeMn} varies with the composition. Tao et al. assumed that the pair potential energy interaction parameters $(\epsilon_{MnFe} - \epsilon_{FeFe})/k$ and $(\epsilon_{FeMn} - \epsilon_{MnMn})/k$ were independent of temperature. The interaction values of B_{MnFe} , B_{FeMn} , θ_{MnFe} , and θ_{FeMn} in liquid Mn-Fe binary alloys are presented in Table 5.

Table 5. The interaction values of B_{MnFe} , B_{FeMn} , θ_{MnFe} , and θ_{FeMn} in liquid Mn-Fe binary alloys at 177 K.

Element	B_{MnFe}	B_{FeMn}	$(\epsilon_{MnFe} - \epsilon_{FeFe})/k(K)$	$(\epsilon_{FeMn} - \epsilon_{MnMn})/k(K)$
Mn-Fe	0.9619	0.9853	69.8	26.3

3.3. Verification of MIVM in Liquid Mn-Fe-C Alloys

Tao et al. [25,26] derived the variation of activity for each component of an *i-j-k* ternary alloy by assuming that the energy of a *j* atom next to a central *i* atom was the same in the presence or absence of a *k* atom next to the *i* atom. The activity coefficient of each composition in Mn-Fe-C liquid alloys can be expressed using Tao’s formula. Considering the Mn-Fe-C liquid alloy as an *i-j-k* ternary system, the activity coefficients of component *i* (Mn) can be written in the form of Equation (9). A similar expression can be used to describe how the activity coefficients of Fe and C vary with composition.

$$\ln \gamma_i = 1 + \ln\left(\frac{V_{mi}}{x_i V_{mi} + x_j V_{mj} B_{ji} + x_k V_{mk} B_{ki}}\right) - \frac{x_i V_{mi}}{x_i V_{mi} + x_j V_{mj} B_{ji} + x_k V_{mk} B_{ki}} - \frac{x_j V_{mi} B_{ij}}{x_i V_{mi} B_{ij} + x_j V_{mj} + x_k V_{mk} B_{kj}} - \frac{x_k V_{mi} B_{ik}}{x_i V_{mi} B_{ik} + x_j V_{mj} B_{jk} + x_k V_{mk}} - \frac{1}{2} \left(\frac{Z_i(x_j B_{ji} + x_k B_{ki})(x_j B_{ji} \ln B_{ji} + x_k B_{ki} \ln B_{ki})}{(x_i + x_j B_{ji} + x_k B_{ki})^2} + \frac{Z_j x_j B_{ij} [(x_j + x_k B_{kj}) \ln B_{ij} - x_k B_{kj} \ln B_{kj}]}{(x_i B_{ij} + x_j + x_k B_{kj})^2} + \frac{Z_k x_k B_{ki} [(x_j B_{jk} + x_k) \ln B_{ik} - x_j B_{jk} \ln B_{jk}]}{(x_i B_{ik} + x_j B_{jk} + x_k)^2} \right). \tag{9}$$

In order to assess the properties of the ternary liquid, such as C solubility and the activity of Mn, Fe, and C, the parameters of the MIVM for the Mn-Fe-C ternary liquid phase are based on the interaction parameters in Mn-C, Fe-C, and Mn-Fe binary alloys.

3.3.1. Evaluation of B_{FeC} and B_{CFe} in Mn-Fe-C Ternary System

In the previous sections, the thermodynamic properties of Mn-C and Mn-Fe in Mn-Fe-C liquid alloys were assessed using MIVM. The Fe-C system was most extensively examined because Fe metal serves as a reservoir for Mn formed via MnO reduction with limited manganese vaporization losses [5]. The interaction parameters between elements in Mn-based alloys are different from those in Fe-based alloys [1–3]. According to previous experimental studies, a series of carbon-saturated compositions in Mn-Fe-C alloy systems were chosen with X_{Fe} and X_C ranging from 0.0 to 0.7 and 0.3 to 0.2, respectively. Activity coefficients of C for all chosen compositions were calculated using Equation (9). The

validity of these parameters was assessed by calculating the carbon activity in Mn-Fe-C alloys at different iron concentrations. The interaction parameters of B_{FeC} and B_{CFe} and the behaviors of carbon in the iron-based binary system were not assessed using MIVM. Figure 5 shows the activity of C in the Mn-Fe-C ternary alloys as obtained by different authors. The interaction parameters B_{FeC} and B_{CFe} obtained through calculation are listed in Table 3. The solubility of C in the Mn-Fe-C melt decreased as the Fe content increased. The activity coefficients of C were determined at various compositions and temperatures up to saturation ($a_C \approx 1$) as a function of the experimentally determined C solubility [5,31].

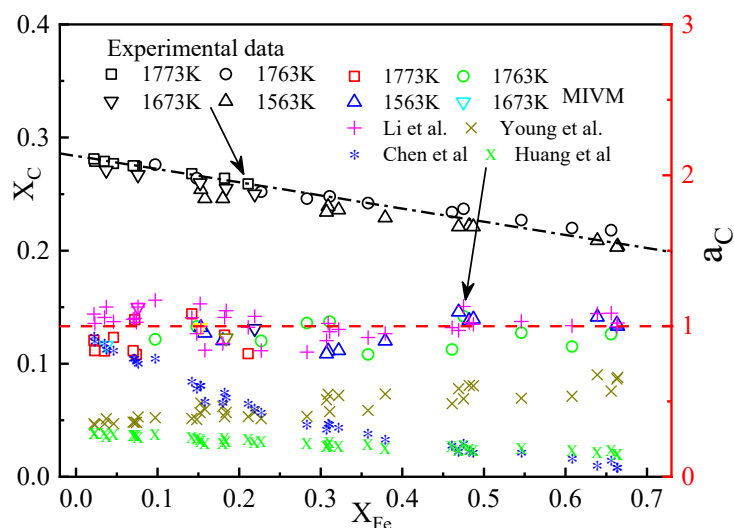


Figure 5. Calculated activity of C in liquid Fe-Mn-C alloys in equilibrium with graphite at various temperatures; experimental data were sourced from [7,8].

Young et al. [12] utilized the lattice site ratio model developed by Chipman [32,33] to describe the activity of C in Mn-Fe-C ternary alloys, showing a negative deviation from ideal behavior at 1563 K to 1773 K. Furthermore, they also described the solution properties of Mn-Fe-C systems using UIPM, obtaining activity values for C of ~ 20 at different iron concentrations. Ni et al. [9] calculated the activity interaction coefficients of C in Mn-Fe-C melt using the same activity method and Wagner's formula, showing a negative deviation between ideal behavior and the calculated value. Li et al. [10] calculated the activity of C in Mn-Fe-C systems using UIPF, showing both positive and negative deviations as a function of the widely varying interaction parameters between Mn-based and Fe-based systems. The interaction parameters for Fe-based alloys were calculated by Young et al. [12], Chen et al. [13,14], and Li et al. [10] as a function of the parameters between Mn and C using UIPM. The relationship between a_C and the content of C and Fe was established at each temperature using Equation (9), and the results are shown in Figure 5. The values calculated for B_{FeC} and B_{CFe} at specific temperatures are presented in Table 6.

Table 6. Interaction parameters of B_{CFe} and B_{FeC} in liquid Mn-Fe-C ternary alloys.

T/K	1563 K	1673 K	1723 K	1763 K	1773 K
B_{FeC}	22.38	22.84	21.60	20.17	24.94
B_{CFe}	1.36	1.86	1.85	3.41	1.38

3.3.2. Activity Coefficient of Mn, Fe, and C in Liquid Fe-Mn-C

The previous section revealed that the interaction parameters of carbon in liquid manganese can be used to describe the thermodynamic properties of ferromanganese alloys. In particular, they allow accurately assessing both Mn activity and C activity in Mn-C alloys. The present study used by the molecular interaction volume model (MIVM) to

predict the thermodynamic properties of Mn-Fe-C ternary alloy through a comparison with experimental data. The activity of C in the Mn-Fe-C melt was calculated experimentally using Equation (9), as presented in Figure 5. The activity of carbon in the liquid Mn-Fe-C system was determined by Li et al. [10], Young et al. [12], Chen et al. [13,14], and Huang et al. [29]. The solubility of carbon increased progressively as Fe was gradually replaced by Mn in Mn-Fe-C liquid alloys. Obviously, all measured carbon activity data fell in the range predicted by different models across the studies composition range in Mn-Fe-C alloys, $X_{Mn} = 0.1$ to 0.7. Accordingly, the activity of carbon was determined at C saturation ($\ln(a_C) \approx 0$) at various compositions and temperatures, while the activity values of carbon were determined using UIPM and MIVM when Fe was replaced completely by Mn. The activity of carbon produced using the lattice site ratio model by Young et al. was usually low at 1673 K to 1773 K. Ni et al. calculated the activity of carbon in Mn-Fe-C melt using the same activity method and Wagner's formula, showing a negative deviation at C saturation ($a_C \approx 1$). Chen et al. calculated the relationship between other thermodynamic properties and temperature using the Gibbs-Duhem relationship, showing that the solubility of carbon increased progressively as Fe was replaced by Mn in Mn-Fe-C liquid alloys. However, the activity of carbon in the temperature range of 1573 K to 1773 K calculated in previous work showed slight deviation from the experimental results. As seen in Figure 6A,B, the activity of C in Mn-C and Mn-Fe-C alloys was well represented when the results were calculated using interaction parameters obtained from MIVM. When using this model, the interaction between C and its first nearest neighbors, Mn and Fe, can be taken into account.

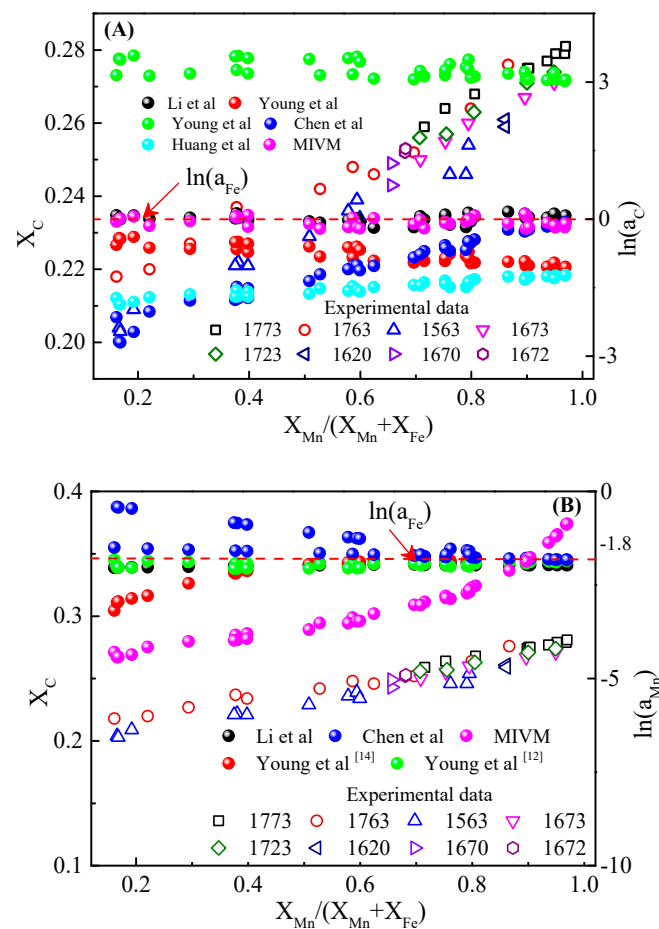


Figure 6. Cont.

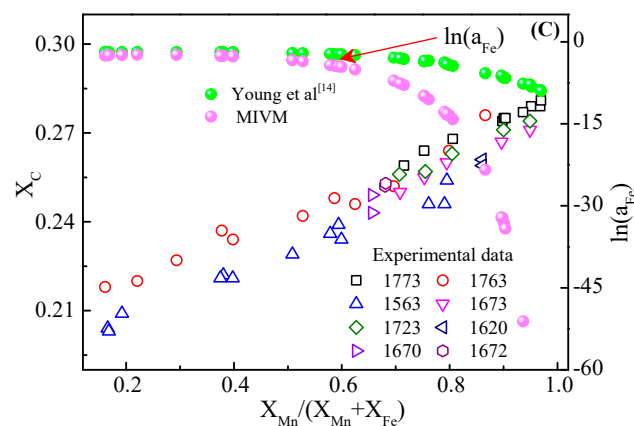


Figure 6. Mn (A), Fe (B), and C (C) activity calculated at different proportions of $X_{Mn}/(X_{Mn} + X_{Fe})$ in Mn-Fe-C liquid alloys in equilibrium with graphite at various temperatures; experimental data were sourced from [7,8,27–31,34].

An assessment of the refining process of high-carbon ferromanganese alloy requires information on the activity of Mn and Fe. The activity of Mn and Fe in Mn-Fe-C liquid alloys was assessed by MIVM using Equation (9) and compared with the experimentally activity of Mn and Fe in Figure 6B,C determined in previous work. As indicated by other models, iron had little effect on the thermodynamic properties of manganese and carbon in Mn-Fe-C alloys. However, the calculated results of MIVM showed that the activity of Mn increased as Fe was replaced by Mn in Mn-Fe-C liquid alloys, indicating that iron had a great influence on the activity of Mn and little effect on the activity of carbon. Upon decreasing X_{Fe} in Mn-Fe-C liquid alloys, the activity of Mn increased, confirming a strong interaction between iron and manganese. This was also verified in [20]. Figure 6C shows the activity of Fe in Mn-Fe-C alloys. Unfortunately, few studies have described the solution properties of iron in the Mn-Fe-C systems. Young et al. [12] utilized the lattice site ratio model developed by Chipman [33] to describe the activity of Fe in Mn-Fe-C ternary alloys, showing that the solution behavior of Fe was not identical to that of Mn.

Figure 7 shows that the environment of each atom in Mn-Fe-C liquid alloys can be determined from MIVM modeling of the ternary alloys, where it can be seen that the environment of carbon is quite different from that of Mn and Fe. If the observed trend is representative of the thermodynamic properties of each component in the Mn-Fe-C ternary alloy in Figure 6, the calculated results of the activity of Mn and C in the binary systems Mn-C and Fe-C would be quite different using MIVM. When both elements are present in the ternary alloy, the interaction between Mn and Fe probably affects the strength of the interaction between carbon and its neighbors, Mn and Fe, thereby forcing the B_{MnC} and B_{FeC} to change under different compositions. This suggests that Mn-Mn and Mn-C interactions become more favorable than Fe-C interactions at high Mn content in Mn-Fe-C ternary alloy. In contrast, Fe-Mn and Fe-C dominate at high Fe content in Fe-Mn-C ternary alloy. This can explain why the activity of Mn increased as Fe was replaced by Mn in Mn-Fe-C liquid alloys, confirming that Fe has a great influence on the activity of Mn and little effect on the activity of carbon [5]. MIVM is able to effectively calculate the activity of individual components in the whole system, which is a feature absent from other models. A significant advantage of MIVM is its ability to explain the experimental phenomenon in Mn-Fe-C ternary systems, whereby the predicted values are in good agreement with the experimental data, showing that the model is reliable, convenient, and economic.

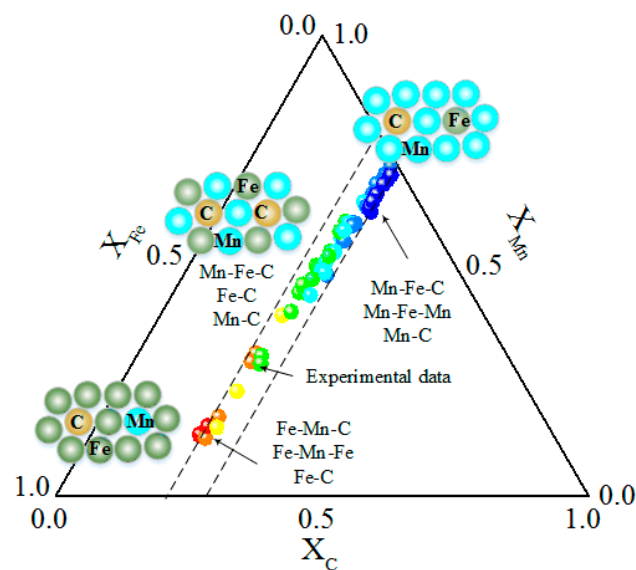


Figure 7. Environment of each atom in Mn-Fe-C liquid alloys determined from MIVM modeling of the ternary alloys.

4. Conclusions

The MIVM parameters for Mn-based alloys were assessed using carbon solubility and activity data for binary and ternary manganese alloys. These parameters were successfully applied to predict the activity of each element in Mn-based alloys, namely, Mn-C, Mn-Fe, and Mn-Fe-C systems. The present assessment by MIVM agreed reasonably with most experimental data and other assessments. The temperature dependence of the interaction coefficients in MIVM was verified in the case of Mn-C and Mn-Fe-C alloys across the studied temperature range.

MIVM takes into account the strong interaction between the metals (Fe, Mn) and nonmetal (C) in Mn-Fe-C alloys, compared with previous thermodynamic modeling, confirming a strong interaction between Fe and Mn. The results calculated by MIVM showed that the activity of Mn increased as Fe was replaced by Mn in Mn-Fe-C liquid alloys, indicating that iron has a great influence on the activity of Mn and little effect on the activity of carbon. The interaction between Mn and Fe is not completely negligible. MIVM can be used to replace other theoretical models due to its clearer physical meaning and more credible extrapolation. A significant advantage of MIVM is its ability to explain the experimental phenomenon in Mn-Fe-C ternary systems, whereby the predicted values are in good agreement with the experimental data, showing that the model is reliable, convenient, and economic.

Author Contributions: L.G., methodology, investigation, and visualization; H.C., writing—original draft and writing—review and editing; W.Z., methodology, investigation, data curation, and software; Z.H., formal analysis and visualization; J.Z., funding acquisition and project administration. All authors read and agreed to the published version of the manuscript.

Funding: This research was funded by the National Natural Science Foundation of China (52074150, 52104332) and the University of Science and Technology Liaoning Talent Project Grant (No. 601011507-05).

Institutional Review Board Statement: The study did not require ethical approval. No special declaration is required.

Informed Consent Statement: The study did not involve humans. No special declaration is required.

Data Availability Statement: The details of our data are presented in the full text. In addition, we have no links to publicly available datasets.

Conflicts of Interest: No conflict of interest exists in the submission of this manuscript, and manuscript is approved by all authors for publication.

References

1. Suh, D.-W.; Kim, S.-J. Medium Mn transformation-induced plasticity steels: Recent progress and challenges. *Scr. Mater.* **2017**, *126*, 63–67. [\[CrossRef\]](#)
2. Djurovic, D.; Hallstedt, B.; Von Appen, J.; Dronskowski, R. Thermodynamic assessment of the Mn–C system. *Calphad* **2010**, *34*, 279–285. [\[CrossRef\]](#)
3. You, B.-D.; Lee, B.-W.; Pak, J.-J. Manganese loss during the oxygen refining of high-carbon ferromanganese melts. *Met. Mater.* **1999**, *5*, 497–502. [\[CrossRef\]](#)
4. Paek, M.-K.; Pak, J.-J.; Kang, Y.-B. Phase equilibria and thermodynamics of Mn–C, Mn–Si, Si–C binary systems and Mn–Si–C ternary system by critical evaluation, combined with experiment and thermodynamic modeling. *Calphad* **2014**, *46*, 92–102. [\[CrossRef\]](#)
5. Coetsee, T.; Reinke, C.; Nell, J.; Pistorius, P.C. Reduction mechanisms in manganese ore reduction. *Metall. Mater. Trans. B* **2015**, *46*, 2534–2552. [\[CrossRef\]](#)
6. Joo, S.-W.; Hong, S.-H.; Lee, G.-H.; You, B.-D. Evaporation behavior of low carbon ferromanganese alloy melt at reduced pressure. *Met. Mater. Int.* **2013**, *19*, 585–590. [\[CrossRef\]](#)
7. Kim, E.-J.; You, B.-D.; Pak, J.-J. Thermodynamics of carbon in liquid manganese and ferromanganese alloys. *Mater. Trans. B* **2003**, *34*, 51–59. [\[CrossRef\]](#)
8. Katsnelson, A.; Tsukihashi, F.; Sano, N. Determination of manganese and carbon activities of Mn–C melts at 1628 K. *ISIJ Int.* **1993**, *33*, 1045–1048. [\[CrossRef\]](#)
9. Ni, R.; Ma, Z.; Wei, S. Thermodynamics of Mn–Fe–C and Mn–Si–C system. *Steel Res.* **1990**, *61*, 113–116. [\[CrossRef\]](#)
10. Li, H.; Morris, A. Evaluation of unified interaction parameter model parameters for calculating activities of ferromanganese alloys: Mn–Fe–C, Mn–Fe–Si, Mn–C–Si, and Mn–Fe–C–Si systems. *Metall. Mater. Trans. B* **1997**, *28*, 553–562. [\[CrossRef\]](#)
11. Djurovic, D.; Hallstedt, B.; Von Appen, J.; Dronskowski, R. Thermodynamic assessment of the Fe–Mn–C system. *Calphad* **2011**, *35*, 479–491. [\[CrossRef\]](#)
12. Lee, Y.E. Thermodynamic assessment of liquid Mn–Fe–C system by unified interaction parameter model. *ISIJ Int.* **2003**, *43*, 144–152. [\[CrossRef\]](#)
13. Chen, E.; Wang, S. Thermodynamic properties of Mn–C melts. *J. Iron Steel Res. Int.* **2008**, *15*, 1–6. [\[CrossRef\]](#)
14. Lee, Y.E. Thermodynamic assessment of liquid Fe–Mn–C system. *Metall. Mater. Trans. B* **1998**, *29*, 397–403. [\[CrossRef\]](#)
15. Pelton, A.D.; Bale, C.W. A modified interaction parameter formalism for non-dilute solutions. *Metall. Mater. Trans. A* **1986**, *17*, 1211–1215. [\[CrossRef\]](#)
16. Bale, C.W.; Pelton, A.D. The unified interaction parameter formalism: Thermodynamic consistency and applications. *Metall. Trans. A* **1990**, *21*, 1997–2002. [\[CrossRef\]](#)
17. Shin, J.P.; Lee, Y.E. Assessment of Mn–Fe–Si–C melt in unified interaction parameter formalism. *Metall. Mater. Trans. B* **2016**, *47*, 216–227. [\[CrossRef\]](#)
18. Kim, M.-S.; Kang, Y.-B. Thermodynamic modeling of the Fe–Mn–C and the Fe–Mn–Al systems using the Modified Quasichemical Model for liquid phase. *J. Phase Equilib. Diffus.* **2015**, *36*, 453–470. [\[CrossRef\]](#)
19. Poizeau, S.; Sadoway, D.R. Application of the molecular interaction volume model (MIVM) to calcium-based liquid alloys of systems forming high-melting intermetallics. *J. Am. Chem. Soc.* **2013**, *135*, 8260–8265. [\[CrossRef\]](#)
20. Ping Tao, D. Prediction of activities of three components in the ternary molten slag CaO–FeO–SiO₂ by the molecular interaction volume model. *Metall. Mater. Trans. B* **2006**, *37*, 1091–1097. [\[CrossRef\]](#)
21. Newhouse, J.M.; Poizeau, S.; Kim, H.; Spatocco, B.L.; Sadoway, D.R. Thermodynamic properties of calcium–magnesium alloys determined by emf measurements. *Electrochim. Acta* **2013**, *91*, 293–301. [\[CrossRef\]](#)
22. Yang, H.; Yang, B.; Xu, B.; Liu, D.; Tao, D. Application of molecular interaction volume model in vacuum distillation of Pb-based alloys. *Vacuum* **2012**, *86*, 1296–1299. [\[CrossRef\]](#)
23. Liu, K.; Wu, J.; Wei, K.; Ma, W.; Xie, K.; Li, S.; Yang, B.; Dai, Y. Application of molecular interaction volume model on removing impurity aluminum from metallurgical grade silicon by vacuum volatilization. *Vacuum* **2015**, *114*, 6–12. [\[CrossRef\]](#)
24. Tao, D.P. Prediction of the thermodynamic properties of solutes in Pb-based dilute solutions. *Thermochim. Acta* **2002**, *385*, 5–10. [\[CrossRef\]](#)
25. Tao, D.P. Prediction of the thermodynamic properties of solutes in the Bi-based ternary dilute solution. *Metall. Mater. Trans. B* **2002**, *33*, 502–506. [\[CrossRef\]](#)
26. Tao, D.P. Prediction of activities of all components in the lead-free solder systems Bi–In–Sn and Bi–In–Sn–Zn. *J. Alloys Compd.* **2008**, *457*, 124–130. [\[CrossRef\]](#)
27. Yan, W.; Yang, Y.; Chen, W.; Barati, M.; McLean, A. Thermodynamic assessment of Si–P and Si–Fe–P alloys for solar grade silicon refining via vacuum levitation. *Vacuum* **2017**, *135*, 101–108. [\[CrossRef\]](#)
28. Huang, W. Thermodynamic Assessment of the Mn–C System. *Scand. J. Metall.* **1990**, *19*, 26–32. [\[CrossRef\]](#)
29. Witusiewicz, V.T.; Sommer, F.; Mittemeijer, E.J. Enthalpy of formation and heat capacity of Fe–Mn alloys. *Metall. Mater. Trans. B* **2003**, *34*, 209–223. [\[CrossRef\]](#)
30. Huang, W. A thermodynamic assessment of the Fe–Mn–C system. *Mater. Trans. A* **1990**, *21*, 2115–2123. [\[CrossRef\]](#)
31. Ahn, S.H.; Kim, Y.H.; Shin, J.-P.; Lee, Y.E. Thermodynamic assessment of liquid Fe–Si–C system by unified interaction parameter model. *ISIJ Int.* **2014**, *54*, 750–755. [\[CrossRef\]](#)

32. Chipman, J. Activity of interstitial and nonmetallic solutions in dilute metal solutions-lattice ratio as a concentration variable. *Aime Met. Soc. Trans.* **1967**, *239*, 1332–1336.
33. Chipman, J. Thermodynamics of liquid Fe-C solutions. *Metall. Trans.* **1970**, *1*, 2163–2168. [[CrossRef](#)]
34. Tanaka, A. Activities of Manganese in Mn-Fe-C, Mn-Si-C and Mn-Fe-Si-C Melts at 1673 K. *Trans. Jpn. Inst. Met.* **1980**, *21*, 27–33. [[CrossRef](#)]